SEMI-ANNUAL TECHNICAL REPORT

ELECTRICAL and OPTICAL PROPERTIES of AMORPHOUS MATERIALS*

by

A Solid-State Group of the Physics Department
Northern Illinois University
DeKalb, Illinois 60115

*Sponsored by
Advanced Research Projects Agency
ARPA Order No. DA-ARO-D-31-124-70-G77

GENERAL INFORMATION

ARPA Order Number	1562
Program Code Number	ϕD1ϕ
Name of Contractor	U. S. Army Research Office
Effective Date of Contract	June 1, 1970
Contract Expiration Date	May 31, 1971
Amount of Contract	$45,868.00
Contract Number	DA-ARO-D-31-124-70-G77
Principal Investigator Phone Number	Dr. Charles Wood (815) 753-1773

CONTENTS

SUMMARY

The theoretical and experimental aspects of the project have been closely coordinated in keeping with the underlying philosophy of this project. Substantial progress has been made theoretically on the development of the Kramers-Krönig (Hilbert) transforms and their application to optical data. Kramers-Krönig analysis of optical reflectivity data has been used extensively in the literature although the reliability of this analysis until now has been questionable. We are now in a position to analyze optical reflectivity data on single crystals and thin films, and determine the fundamental optical constants, n and k, with a reliability and accuracy well beyond that available in the past.

In addition, computer programs are under development which will delineate the optimum experimental conditions and will perform analysis of the optical constants of thin films from transmission data.

Basic to this program is a comparison of the properties of materials in single crystal and amorphous form. The growth of large single crystals of several compounds and their solid solutions has been successfully accomplished and a considerable amount of optical data has been amassed on these crystals.

A very significant finding has been that the standard method of preparing the amorphous forms of the Group V-VI compounds by vacuum evaporation from the compound is very unreliable from the compositional viewpoint. It appears probable that no data has ever been reported on truly "Sb_2Se_3" amorphous films, despite considerable literature on the subject. Several approaches have been taken, or are under development, which have yielded amorphous Sb_2Se_3 films.

Initial Mossbauer studies have shown that the Sb atoms in amorphous Sb_xSe_y ($x < 2$, $y > 3$) films differ in environment from the single crystal form and therefore appear to be amorphous rather than microcrystalline.

Highlights in the optical studies to date are: the band gap in Sb_2Se_3 appears to be due to a direct transition; plasma resonance frequencies can be accurately determined by thermoreflectance data; photon counter techniques show great promise in determining the critical points in band structure; measurement of the phase shift between the incident radiation and the photoresponse is a powerful technique for determining the spectral dependence of lifetime and thus can yield fundamental data on differences between the amorphous and single crystal forms of a material (eg. Se); contacts do not influence the spectral response of Sb_2Se_3 provided that they are shielded from the incident radiation.

We feel that a good start has been made in the past four months on a broad systematic approach toward the understanding of the electrical and optical properties of the Group V-VI amorphous semiconductors. A better understanding of the basic properties of these amorphous materials should lead to improved, more reliable and new device applications.

THEORETICAL RESEARCH

The theoretical research accomplished during the first four months of the contract period has been substantial. The work on Kramers-Krönig (Hilbert) transforms is essentially complete and is to be detailed in two papers, the first of which is now being submitted for publication (Appendix 1). The second, which contains the specifics of applying the technique to optical properties, i.e. to obtaining the optical functions of a system from normal incidence reflectivity data is in preparation for submission. It appears that the method of carrying out Kramers-Krönig transforms which has been adopted in this work is extremely accurate and that it can be of great value for the analysis of data as well as for obtaining Hilbert transforms which are of interest in applied solid-state theory such as those of densities of states calculated by Monte-Carlo techniques. These are of interest in impurity problems.

There is underway another effort dealing with analysis of optical data. In this instance we are attempting to construct computational techniques to extract the optical constants of thin films upon non-absorbing substrates from normal-incidence reflectivity and transmissivity measurements. This is a problem which has, in our opinion, never been satisfactorily resolved although much effort has been expended toward its solution. It appears that measurements upon at least two systems of differing thickness and a fitting technique which includes interference exactly in some spectral regions is necessary for the proper resolution of the optical constants of the thin film materials with which we are concerned. In other spectral regions it appears possible to neglect interference and to sum up the multiple reflections in

intensity in order to find n and k. There are, in addition, spectral regions in which interference is not resolvable and the exact equations may be appropriately averaged. Computational codes for dealing with this important data reduction problem are in development.

There is continuing work on the electronic structure of amorphous solids. The preliminary calculation on Ge indicated that great care must be taken in the construction of ensemble-averaged structure factors for amorhpous systems in order to eliminate spurious energy eigenvalues from the final results (i.e., energy eigenvalues which appear in the solution for the amorphous system but do not converge to the proper solutions in the extreme crystalline limit). Presently the problem is being reformulated in the Wannier (real-space) representation in terms of the real-space pair-correlation function. The same techniques for averaging computationally over an ensemble of lattice configurations are being used. It is expected that this reformulation of the problem will lead to proper behaviour of the solutions in the extreme limits of the crystalline and random lattices.

MATERIALS PREPARATION

A) Single Crystals

No difficulties have been experienced with growing large single crystals of Sb_2Te_3 and Sb_2Se_3. A simple horizontal zone-refiner with background heating to prevent dissociation of the compound during melting is being used to grow the crystals. The shape of the freezing interface can be seen and controlled for self-seeded single crystal growth.

Growth of Sb_2S_3 has proved to be more difficult due to the high dissociation vapor pressure of S over the melt. A vertical zone-refiner and a vertical Bridgman furnace with an extremely sharp temperature gradient have been constructed. It is expected that one of these will prove suitable for the growth of single crystal Sb_2S_3.

B) Amorphous Thin Films

An amorphous thin film can be readily prepared by vacuum evaporation from a source of Sb_2Se_3 on to a room-temperature substrate. This is the standard procedure reported in the literature. However, we have found by chemical and x-ray emission analysis that the resulting compositions of the films deviate considerably from stoichiometry, generally on the Se-rich side and with the composition depending greatly on the temperature of the evaporation boat. Since there is considerable data in the literature on so-called amorphous "Sb_2Se_3" films, it is of considerable interest, therefore, to examine the optical properties of amorphous films of the Sb-Se system as a function of Sb to Se ratio.

The type of apparatus used for our evaporation experiments was developed prior to the contract and is generally described in the attached publication (Appendix 2) with the main difference being that the substrate temperature can

be controlled down to liq. N_2 temperatures by insertion of a copper cold -finger into the system.

We have found that Se is preferentially evaporated at low source temperatures - particularly below the melting point of the source material (mp. of $Sb_2Se_3 \sim 610^oC$). Films approaching stoichiometry have been made by raising the source temperature to 700°C, i.e. well above the melting point and well above that required for fast rates of depositions; but the films, although less Se rich than at lower temperatures, were still in the range Sb_xSe_y (where $x << y$). The results suggest that Sb_2Se_3 does not evaporate as a molecular species. However, the lack of stoichiometry in the films may be partly a sticking coefficient problem; thus a comparison of composition as a function of substrate temperature will be tried and should help elucidate this effect.

Currently, experiments are underway to use large evaporation sources rich in Sb, eg. SbSe, and to examine the stoichiometry of the films as a function of subsequent depositions keeping the source temperature fixed at $\sim 650^oC$. Initial results show some success by this approach. A thick film ($\sim 20\mu$) of Sb_2Se_3 composition has been prepared and will be used in the Mossbauer experiments.

An alternative approach to obtain stoichiometric films is being tried, namely, coevaporation of Sb and Se in an ion-pumped bell-jar system with the relative rates of evaporation being controlled by quartz-crystal oscillators. Early difficulties in rate fluctions appear now to be resolved and again early indications are that films of controlled stoichiometry can be prepared by this technique.

A third approach to be tried is to prepare amorphous films by sputtering, and a system has been designed to accomplish this. Correspondence between

source and deposited film is expected by first allowing equilibrium conditions to be maintained before exposing the substrate to deposition (1),(2),(3). R. F. Sputtering will be employed to clean the fused quartz substrates before deposition of the film.

C) X-ray Emission Analysis

A Norelco Vacuum X-ray Spectrograph with LiF analyser and Cu-target has been employed to analyse the composition of our evaporated films. The intensities of the $K_{\alpha 1}$ and $K_{\alpha 2}$ lines of Sb and Se were measured to determine the Sb:Se ratio in the films. This is not a reliable absolute method of analysis and therefore it is essential to prepare standards for analysis and, because of reabsorption of the characteristic emmitted x-rays, it is essential that these standards are of a form closely approximating to that of the material to be analyzed.

Standards for analysis were prepared by heating weighed amounts of Sb and Se in a flat-bottomed evacuated quartz capsule placed in a rocking furnace. The charge was quenched onto the flat-bottom section and thus approximated in geometry to the thin evaporated film samples. Despite extreme quenching conditions (i.e. quenching into a super-saturated salt-water solution held near solid CO_2 temperatures) the resulting discs of Sb_xSe_y compositions were always crystalline showing that vapor quenching is much more effective in producing amorphous material. Since the x-ray emission intensities are thickness dependent, reliable analysis can only be obtained on very thick or very thin samples.

STRUCTURAL INVESTIGATIONS

A) Mossbauer Studies

Mossbauer studies using a high intensity Sb source have been carried out* on two powdered samples of single-crystal Sb_2Se_3 and on two amorphous films of Sb_xSe_y, vacuum deposited onto fused quartz substrates. Very thick ($\sim$ tens of microns) samples of Sb_xSe_y were prepared for these experiments in order to obtain the optimum content of 5 mg of Sb per cm^2 for these measurements. Difficulty experienced in the thick films peeling from the substrate was overcome by reducing the size of the source aperture thus slowing the evaporation rate.

The single crystal samples showed Mossbauer spectra which could be fitted only by postulating two sites for the Sb atoms, which is consistent with crystallographic data. For the amorphous films a single Sb site fit was obtained showing that the very short range order differs significantly in the amorphous form, i.e. the films cannot be regarded as microcrystalline. It should be noted that these films were of the conventional amorphous variety i.e. non-stoichiometric composition. A further thick film sample has been prepared which appears from x-ray emission data to be Sb_2Se_3 and this will be Mossbauer analyzed shortly.

A further Mossbauer study, to be carried out in our laboratories, has been designed to clarify the role of Sn in $As_2Se_3Sn_x$-glasses on the composition dependence of electrical conductivity and microhardness. A model in which a $SnSe_2$-type bond is replaced by a SnSe-type bond, as the concentration of tin increases, has been postulated by Shkol'nikov (4) to explain hardness and conductivity changes. Borisova et al (5) conclude in a recent Mossbauer study that the only Sn^{4+} occurs and that Sn is bonded only to Se; however, an examination of their data leads us to conclude that a distribution of ionic states is present which

---

* In collaboration with Dr. Stan Ruby of Argonne National Laboratory.

could, in fact, be that predicted by Shkov'nikov. Further, Borisova et al do not find the correlation of intensity with coordination number previously found in glasses.(6) The Mossbauer experiments on $As_2Se_3Sn_x$-glasses will be repeated with narrower source lines and better statistics to determine the degree of local order and the distribution of ionic states of Sn. A test of the relationship of Mossbauer intensity to coordination will also be made.

B) X-ray Studies

The experimental equipment consisting of a Laue camera, a Weissenberg and precession camera, in connection with a Norelco generator, has been set up for investigating the $Sb_2Te_{3-x}Se_x$ system. In addition to verifying and possibly refining the exact structure of Sb_2Te_3 by x-ray data, it is of particular interest, to study the changes in the structure due to incorporation of Se atoms. The question of the specific ordering is of great importance since it has a strong influence on the transport properties.

According to Teramoto and Takayangi (7) in the $Sb_2Te_{3-x}Se_x$ solid solutions 2/3 of all Te atoms can be replaced by Se without changes of the rhombohedral (hexagonal) structure. Due to the smaller atomic radius of Se, the lattice dimensions of a and c decrease with increasing amounts of Se. When 2/3 of the Te atoms are replaced by Se, the lattice constant change amounts to about 4% for a and 3% for c. The antimony may go into either the c or a positions or be statistically distributed into both. Since the atomic scattering factors of Te and Se vary considerably, the scattering amplitude will differ considerably for these various possibilities. Once the correct model is established, the parameters can be refined by a least squares method using the intensities of all reflections. Changes of inter-atomic distances will be correlated with transport properties.

OPTICAL PROPERTIES

Work related to this program on the properties and growth of Group V-VI compounds was already underway before the commencement of this contract. In particular, a large amount of work on the growth of single crystals of Sb_2Te_3 - Sb_2Se_3 solid solutions together with the measurements of their optical properties, was nearing completion. However, analysis of the data was carried out under the contract and the results of this work have been accepted for publication (Appendix 3).

A) Reflectivity

The optical reflectance and transmission of single crystal specimens of solid solutions of the $Sb_2Te_{3-x}Se_x$ compounds were investigated in the photon energy range 0.04 eV to 6.5 eV. A wide range of solid solutions from x = 0 to 2 were prepared all having rhombohedral structure and were found to exhibit properties closely corresponding to the isostructural compounds Be_2Te_3, Bi_2Se_3. Small indirect band gaps approaching semimetallic values were obtained for all compositions. The high free-carrier concentrations gave rise to plasma effects in the near infra-red. The chemical bonding concepts applied to similar systems seemed applicable with only slight modification.

A result of some significance to this program was that both the reflectivity and transmission data show that the absorption edge of orthorhombic Sb_2Se_3 corresponds to direct transitions, at least for non-polarized light perpendicular to the cleavage plane, i.e. with the electric vector parallel to the (a) and (c) directions. This is in contrast to the assignment of an indirect transition by Shutov et. al. (8) and is of utmost importance for future comparisons of the band structure of Sb_2Se_3 in the amorphous and crystalline form.

Experiments are currently underway to measure the reflectivity and

transmission data as a function of polarized light in the three primary crystallographic orientations of Sb_2Se_3. Some difficulty has been experienced in preparing good reflectivity surfaces cut perpendicular to the cleavage plane, or thin optical transmission samples of the same orientation, due to the propensity of the crystals to cleave easily. An encapsulation technique in a polyester casting resin shows some promise of overcoming this difficulty. The suitability of various chemical etches for preparing surfaces for reflectivity measurements has also been investigated. For Sb_2Se_3.. 2 parts HCl: 1 part H_2O_2 by volume has been found to produce a satisfactory surface; and for Sb_2Te_3, the best etch appears to consist of 14 parts Acetic Acid (saturated with Citric Acid) 1 part Bromine.

Although no difficulties have been experienced in preparing good amorphous thin film specimens for optical measurement, work has been held up in this area mainly by lack of control of stoichiometry of the films (see Preparative Section) and by lack of a suitable analytical techniques to accurately obtain the n and k values for comparison with data on single crystals (see Theory Section).

B) Thermally modulated reflectivity

The thermally modulated reflectivity of single crystalline materials $Sb_2Te_{3-x}Se_x$ ($x = 0 - 2$) was measured in the UV, visible and IR region. Experiments were performed in the IR region (8-28μ) in order to confirm the existence of plasma resonance of free holes. The reflectivity structure due to this resonance was rather broad due to strong free-carriers absorption and interband (light and heavy hole bands) transitions, which mask the resonance effect. However, the thermal modulation gave precisely the resonance frequencies ω_p. The knowledge of this resonance frequency ω_p together with the Hall coefficient and resistivity can determine the optical effective mass and

the relaxation time due to free-carrier-phonon scattering. This data has been submitted for publication (see Appendix 4).

The thermomodulated reflectivity was also performed for Sb_2Te_3 in the visible and near UV region using a modified Cary 14R spectrophotometer to confirm the existence of critical points corresponding to transitions at points of high symmetry in the Brillouin zone. Preliminary results yield quite sharp structure which indicates agreement with identification of these critical points in the work of Sobolev et al. (9) from low temperature reflectivity measurements. The structure of the thermomodulation spectrum agrees with the photon counter (see Transmission measurements).

So far it has been found difficult to extend measurements beyond the region 3000A to 7000A^o due to cut-off of the photomultiplier and to low light intensity in the UV region. These problems are expected to be solved using the RCA C31015C "Quantacon" photomultiplier having an extended response from 2000 to 9000A^o and using the McPherson 225 Vacuum UV monochromator. The $Sb_2Te_{3-x}Se_x$ compounds are very suitable for the thermomodulated spectroscopy for x = 0 to 2 due to their low resistivity. However, for x > 2, the thermomodulation is difficult as the resistivity increases with x and other forms of modulations have to be applied. Electric field and/or photomodulation seem to be the most appropriate.

C) Transmission measurements

Direct transmission measurements were performed on thinly cleaved specimens of $Sb_2Te_{3-x}Se_x$ (x = 0 to 3) in the 2000 to 10,000A^o wavelength region. This photon energy range is higher than the direct gap, and because the absorption coefficient is high ($\sim 10^4$ to 10^5 cm^{-1}) in this range, a sensitive detector must be used even for very thin samples ($\sim 1\mu$). Also stringent precautions must be

taken to avoid any stray light. The latter problem was successfully solved using an O-ring sealed vacuum-tight blackened tube with the sample sealed inside. Using a photon counter, a transmission of 10^{-7} to 10^{-8} was measured with a S/N ratio of 100/1 to 100/3 provided good stability of the light source was maintained. This set-up is expected to be improved using a double beam method, i.e. a double-channel photon-counter with an on-line computer.

The transmission spectrum showed fine structure corresponding to critical points in the Brillouin zone in agreement with published data for x = 0 by V. V. Sobolev et al., (9) and for x = 3 by S. D. Shutov et al. (8) Our structure was much sharper than that obtained by the above investigators, even in comparison with their low temperature reflectivity data.

A sharp transmission window at $\sim$2,800A^{o} was shown by all samples, which coincides with sharp fall of the reflectivity. This effect is probably due to sharp fall-off of the density of states, in agreement with the band model of isostructural Sb_2Te_3 by Borghese and Donato (10) rather than to a plasma resonance of electrons in the valence band. The latter effect is expected to occur at a higher energy range ($\sim$10 - 14 eV) and can provide the coordination number and the degree of ionicity of the bonds.

D) Photoemission

Photoemission measurements can yield the electronic density of states, the electron-electron scattering length and the conservation of the electron momentum can be obtained. The latter is of considerable importance for the study of the difference between amorphous and single crystalline materials as far as the selection rules and the degree of localization of electronic states are concerned.

A special phototube has been designed and is under construction which will allow measurements on freshly cleaved surfaces of single crystals or on

amorphous films evaporated in the ultra-high vacuum of 10^{-9} to 10^{-11} torr. A vacuum UV Monochromator (McPherson 225) will be used as the radiation source. This monochromator has been modified by attaching a Varian 400l/sec noble gas pump to assure oil-free operation, which is a necessary condition for the windowless operation of the light source for energies over 12 eV. The possibility of utilizing the radiation from the Synchrotron at the University of Wisconsin is also being explored.

An electronic circuit has been constructed to measure the photoemission current ($\sim 10^{-11}$ A to 10^{-14}A). The main part consists of a feedback Keithley 604 or 640 electrometer, and a Keithley 82 and a PAR HR - 8 Lock-in amplifier together with a bridge circuit for rejection of the capacitive component of the photoemission current.

E) Photoconductivity

Photoconductivity measurements have been performed with emphasis on optical and transport properties. An experimental technique of measuring the spectral dependence of the lifetime τ of photogenerated carriers was developed which employs a measurement of the phase shift ψ between the square light pulses and the first harmoic frequency of the photocurrent response using a Lock-in amplifier.

This method was applied first to the rather well-investigated element Se in the amorphous and single crystal (trigonal) form at 90^{o}K and 300^{o}K. It was found that the photoconductivity of single crystal of trigonal Se comprises both valence to conduction band transitions as well as transitions from states inside the forbidden gap into the conduction band. In the amorphous Se, only the valence band to conduction band transitions contribute to the photoconductivity. In fact, in amorphous Se the photoconductivity onset occurs at higher energies than the band gap, which has been explained (11) by strong exciton absorption. This work has been submitted for publication (Appendix 5).

Similar results were obtained for amorphous films of Sb_2Se_3 with an excess of Se. While the photoconductivity onset for these films occured either at 0.8μ or at 1.0μ, the absorption edge is located at longer wavelengths (1.2 to 1.3μ). Further experiments on the photoconductivity of stoichiometric amorphous films of Sb_2Se_3 should indicate whether the above effect is due to exciton absorption, similar to case of amorphous Se films, or the light scattering in amorphous films or to optical absorption due to excess Se atoms in non-stoichiometric films.

The photoconductivity of Sb_2Se_3 films was measured using evaporated Au or Sb contracts. The overall spectral response was the same, for both contacts contrary to the work of Lyubin et al. (12) who maintain that Au contacts were blocking and Sb injecting, and that they produce a different photoconductive spectral response. Our optical transmission measurements on Sb_2Se_3 films show an absorption peak at 0.75μ in accordance with (13) and sometimes additional structure at 1.0μ and 0.85μ. Results in (12) may be due to the use of a sandwich structure with unavoidable illumination of contacts producing photovoltaic effects, while in our case contacts were carefully shielded from illumination.

The photoconductivity in orthorhombic single crystals of Sb Se was investigated as a function of polarization of the electrical vector E_o of the incident light with respect to crystallographic axes of the single crystal. E_{drift} was || c with evaporated gold contacts. For this orientation, the photocurrent showed a maximum at 1.05μ and a secondary maximum at 0.75μ. For E || a the first maximum was shifted towards 1.075μ (in accordance with the shift of the absorption edge) while the secondary maximum remained at 0.75μ. Also, another maximum was found at 0.575μ. The secondary maximum at 0.75μ was not reported in earlier work on single crystals (13) but was reported to occur in Sb_2Se_3 amorphous films (13), in agreement with our results.

TRANSPORT PROPERTIES

Hall Effect Measurements

There is some evidence to indicate that inorganic materials with a chain-like crystal structure, e.g. single crystals of selenium (14), exhibit a barrier-type photoconductivity. The photoconductive mechanism in some compounds containing selenium, e.g. PbSe, and related chalcogenides, has long been in contention with the barrier theory receiving strong consideration (15). Since the arsenic and antimony chalcogenides are related structurally and compositionally to the above materials it is essential that methods developed to investigate transport and photoconductive mechanisms will allow one to distinguish between carrier generation and barrier layer theories. A Hall-effect or photo-Hall effect measurement in which the frequency of the applied electric field can be varied up to high values ($\sim$ MHz) will, by virtue of shorting potential barriers, allow this distinction to be made.

Initially, the Hall coefficient for single crystals of selenium will be measured as a function of frequency of the applied electric field. The frequencies used will range of 20 Hz to 1 MHz. The resistivity will also be measured for the same frequency range.

A typical 6 contact Hall sample will be used together with 3 RF switches to measure current, Hall voltage and voltage drop due to resistance. The input signal will be obtained from a Hewlett-Packard oscillator through a RF transformer which has a flat response from 20 Hz to 5 MHz. The actual voltage measurements will be made by a Keithley lock-in amplifier system. Preliminary measurements indicate no distortion of wave form up to 1 MHz and signals as small as 10μ volts have been measured to an accuracy of a few percent.

REFERENCES

(1) M. H. Francombe, Trans. 10th Nat. Vac. Sym., MacMillan 316 (1963)

(2) I. H. Pratt, 10th Conf on Military Electronics (1964)

(3) G. S. Anderson, Wm. N. Mayer, and G. K. Wehner, Jour. Appl. Phys. 33 2991 (1962)

(4) E. V. Shkol'nikov, Chemistry of Solids (in Russian), Leningrad State University (1965), p.199

(5) Z. U. Borisova, L. N. Vasil'ev, P. P. Seregin, and V. T. Shipatov Soviet Physics - Semiconductors Vol. 4, No. 3 (1970)

(6) K. P. Mitrofanov and T. A. Sidorov, Soviet Physics - Solid State Vol. 9, No. 3, (1967)

(7) I. Teramoto and S. Takayanagi, J. Phys. Chem. Solids 19, 124 (1961)

(8) S. D. Shutov, V. V. Sobolev, Y. V. Popov, and S. N. Shestatskii Phys. Stat. Sol. 31, K23 (1969)

(9) V. V. Sobolev, S. D. Shutov, Yu. V. Popov, and S. N. Shestatskii Phys. Stat. Sol. 30, 349 (1968)

(10) F. Borghese and E. Donato, Nuovo Cimento 53B, 283 (1968)

(11) J. L. Hartke, P. J. Regensburger, Phys. Rev. 139A, 970 (1965)

(12) V. M. Lyubin and V. S. Maidzinskii, Soviet Phys. - Semiconductors 3, No. 11, 1408 (1970)

(13) B. T. Kolomiets and A. K. Zeinally, Sov. Phys. Solid State 1, No. 6, 897 (1954)

(14) J. Stuke, Phys. Stat. Solidi 6, 441 (1964)

(15) R. A. Smith, Semiconductors, Cambridge (1961) p.414

FISCAL STATUS

	Amount Budgeted	Amount Expended Sept. 30, 1970	Projected Total Expenditure
Personnel	$ 31,368	$ 10,551.60	$ 20,816.40
Supplies, Expenses & Services	12,000	3,821.28	8,178.72
Travel	2,500	-	2,500
Indirect Costs	11,952	11, 952	

APPENDIX 1

To be Submitted to the Journal of Mathematical Physics

New Method for Kramers-Kronig Transform*†

I. General Formalism and Application To Compact Functions

R. AFSHAR

Department of Physics

Northern Illinois University

DeKalb, Illinois 60115

F. M. MUELLER

Argonne National Laboratory

Argonne, Illinois 60439
and
Department of Physics

Northern Illinois University

DeKalb, Illinois 60115

J. C. SHAFFER

Department of Physics

Northern Illinois University

Dekalb, Illinois 60115

---

*Based on work performed under the auspices of the U. S. Atomic Energy Commission.

†This research was supported by the Advanced Research Projects Agency of the Department of Defense and was monitored by the Army Research Office Durham, under Contract No. DA-ARO-D-31-124-70-G77.

ABSTRACT

It is shown that the Hermite functions form a compact, swiftly convergent representation of the Hilbert transform operator (Kramers-Kronig transform). Application is made to the practically important case of the Hilbert transform of a function non-zero only over a finite region. Hermite functions form a natural expansion set in such cases. If the function to be Hilbert transformed has discontinuous derivatives (critical point structure) at a set of values ω_i, then the transformed function also has discontinuous derivatives at the same set of ω_i. The number and ω position of critical point structure is shown to be invariant to Hilbert transformation. The practical significance of measuring experimental optical data only at the zeros of Hermite polynomials is stressed. The zeros and weight functions for Hermite integration for n = 20, 26, 50, 76, 150, and 300 is given in an appendix.

I. INTRODUCTION

Dispersion relations, starting with the classical work of Kronig[1] and Kramers,[2] have been applied to an ever widening variety of problems in physics. Elegant formalisms[3-5] now exist so that the mathematical structure of the Hilbert transform is fully, and completely understood. The practical application of the Hilbert transform to physics, especially to the analysis of experimental data, has been problematic for two principle reasons: (1) Direct integration of (necessarily) discontinuous data with singular kernels is computationally impossible; (2) Data do not exist over the whole real line ($-\infty < \omega < \infty$), but only over a finite range or, at best, a sequence of overlapping finite ranges. The first problem has generally been treated by "smoothing" the data over a region. If the smoothing was achieved by expanding M data points in a Taylor series to order N ($M > N$), then the smooth function is continuous in its zeroth through Nth derivatives in the region, but discontinuous in the sense that N + 1th and higher derivatives are set equal to zero (Removing information from the Hilbert transform.) At the region boundaries all derivatives are discontinuous. The effect of these discontinuities and forced zeros on the resultant Hilbert transform is generally unknown. This problem is usually solved by making plausibility arguments that if the transform function is smooth and or if applying the Hilbert transform twice returns approximately the negative of the original smoothed function, then the transformation

was successful.

The second problem exacerbates the first. Generally the data are continued above the last data point ω_h by means of a Laurent expansion ($\sim \sum_n a_n \omega_h^n \omega^{-n}$), where a_n are expansion coefficients, and ω is the measured independent variable. Below the first data point a Taylors' series is the expansion set. Again plausibility arguments are used. (We neglect completely in this paper the problem of extrapolation in cases where significant structure exists in an unmeasured region.)

The increased application of Monte Carlo methods to physical models yields numerical results which cannot be represented in closed form. Thus the calculation of the Hilbert transform of such results is also difficult as, for example, in the important case of finding the Hilbert transform of a density of states.

In this paper we consider a mathematically exact treatment of this problem which is simple to use, can be applied to a variety of cases , automatically least-square fits discontinuous data over the entire measured region, provides a natural form of extrapolation function, and in the special case of optical data allows a simultaneous best fit to all of the variables $\epsilon_1(\omega)$, $\epsilon_2(\omega)$, $\ln R(\omega)$, $\varphi(\omega)$ $N(\omega)$, $k(\omega)$, and $T(\omega)$ in terms of <u>one</u> expansion set, where ϵ_1 and ϵ_2 and $N(\omega)$ and $k(\omega)$ are the real and imaginary parts of the dielectric function and the index of refraction respectively, R is the normal reflectivity, φ the phase, and T the fractional transmitted intensity. In Section II we discuss the formal derivation of our technique. In

Section III we give the results of two applications: the Hilbert transform of the density of states of Monte Carlo calculations of a simple cubic s band and face centered cubic palladium. Section IV summarizes our results and discusses application to other systems. The numerical application to the analysis of normal reflectivity data will be detailed in a further publication.

II. FORMALISM

A. The Hilbert Operator

As is well known, the Kramers-Kronig relation between the real and imaginary parts of a response function arise because of causality. If, in the long wave length limit, a time varying field $E(t)$ is impressed upon a media at $t = 0$, then the linear response $D(t)$ must also be zero for $t < 0$, and is given by

$$D(t) = \epsilon(t)\, E(T) \tag{1}$$

where ϵ is the generalized susceptibility. Upon taking the complex Fourier transform of (1) we obtain the Kramers-Kronig relations:

$$\epsilon_1(\omega) - 1 = \frac{P}{\pi} \int_{-\infty}^{\infty} \frac{\epsilon_2(\omega')d\omega'}{\omega' - \omega}$$

$$\epsilon_2(\omega) = -\frac{P}{\pi} \int_{-\infty}^{\infty} \frac{(\epsilon_1(\omega) - 1)d\omega'}{\omega' - \omega} \tag{2}$$

where ϵ_1 and ϵ_2 denote the real and imaginary parts and the 1 comes from the fact that $\epsilon_1(\infty) = 1$. If we regard the principle value integrals of (2) as an operator P then we have the functional relation:

$$(\epsilon_1 - 1) = P(\epsilon_2)$$

$$\epsilon_2 = -P(\epsilon_1 - 1) \tag{3}$$

or that

$$(\epsilon_1 - 1) = -P^2(\epsilon_1 - 1) \tag{4}$$

which makes manifest that P is an antiunitary operator.

To mathematicians the relations (2) form a Hilbert transform pair. The close relationship between Hilbert and Fourier transformations is seen in that the kernel for Fourier transformation is given by

$$K_F(\omega - \omega') = \frac{1}{\pi}\int_0^\infty dt \cos(\omega - \omega')t \tag{5}$$

whereas the kernel for the Hilbert transformation is

$$K_H(\omega - \omega') = \frac{1}{\pi}\int_0^\infty dt \sin(\omega - \omega')t \,. \tag{6}$$

A more familiar form for (5) and (6) is

$$K_F(\omega - \omega') = \delta(\omega - \omega') \tag{7}$$

(a Dirac delta function) and

$$K_H(\omega - \omega') = \pi \frac{P}{(\omega - \omega')} , \tag{8}$$

which we define as

$$K_H(\omega - \omega') \equiv P(\omega - \omega') \tag{9}$$

The relations (5) and (6) form representations of the operators K_F and K_H. Any denumerable, complete set of functions defined over the whole real line may be used to form a representation for (5) since in terms of any complete orthonormal set $\psi_n(\omega)$ we have,

$$\delta(\omega - \omega') = \sum_n \psi_n(\omega)\, \psi_n(\omega') , \tag{10}$$

where the sum extends over all of the members of the set. An analogous representation for the operator $P(\omega - \omega')$ may be constructed as follows:

From (6), or by direct integration we have that P is given by

$$P(\omega - \omega') = \frac{-i}{2\pi} \int_{-\infty}^{\infty} dt\, SGN(t)\, e^{i(\omega - \omega')t} \tag{11}$$

where SGN (t) is the signature or signum function (-1 for $t < 0$ and +1 for $t > 0$ and 0, say, if $t = 0$). We recall that the signum function, like the delta function, is a generalized

function,[4] and has the property that

$$\frac{d}{dx} \text{SGN}\,(x - x') = 2\,\delta\,(x - x') \tag{12}$$

Equation (11) allows us to construct an infinite number of representation of the Hilbert operator by simply finding the representation for exp (iωt) in terms of the complete set and using (11). Here, and for the rest of this paper, we will concentrate on a single representation, the Hermite functions, $\psi_n(\omega)$. We recall[7] that the nth order orthonormal Hermite function is found from the corresponding Hermite polynomial $H_n(\omega)$ by

$$\psi_n(\omega) = N_n\, e^{-\frac{\omega^2}{2}}\, H_n(\omega) \tag{13}$$

where N_n is a normalization factor given by

$$N_n^2 = (2^n\, n!\, \sqrt{\pi})^{-1} \quad . \tag{14}$$

The most important property of the Hermite functions we need is that up to a trivial factor i^n, the Fourier transform of a Hermite function of order n, is the same Hermite function:

$$\frac{1}{\sqrt{2\pi}} \int_{-\infty}^{\infty} e^{i\omega' t}\, d\omega'\, \psi_n(\omega') = i^n\, \psi_n(t) \quad . \tag{15}$$

Multiply both sides of Eq. (15) by $\psi_n(\omega)$, and utilizing eq. (10), we have a representation for $e^{i\omega t}$:

$$e^{i\omega t} = \sqrt{2\pi} \sum_n i^n \psi_n(t) \psi_n(\omega) \; ; \qquad (16)$$

and $e^{-i\omega' t}$

$$e^{-i\omega' t} = \sqrt{2\pi} \sum_m (-i)^m \psi_m(t) \psi_m(\omega') \qquad (17)$$

Placing (16) and (17) in (11) we have that

$$P(\omega - \omega') = (-i) \sum_n \sum_m (i)^n (-i)^m \psi_n(\omega) \psi_m(\omega') S'_{nm} \qquad (18)$$

where S'_{nm} is given by

$$S'_{nm} = \int_{-\infty}^{\infty} dt \; SGN(t) \psi_n(t) \psi_m(t) \quad . \qquad (18)$$

We notice that S'_{nm} forms the representation of the signum operator in terms of the Hermite functions. We recall that the Hermite functions are simply odd or even by the rule: $\psi_n(-t) = (-1)^n \psi_n(t)$. The integral for negative t may be reduced to

$$S''_{nm} = (-1)^{m+n+1} \int_o^{\infty} d\rho \; \psi_n(\rho) \psi_m(\rho) \qquad (19)$$

so that the whole integral is given by:

$$S'_{nm} = [1 + (-1)^{m+n+1}] \int_o^{\infty} dt \; \psi_n(t) \psi_m(t) \qquad (20)$$

Eq. (20) makes clear that S'_{nm} is zero unless n + m is odd. Let us assume that this is true. Then (20) may be written

$$S'_{nm} = 2 \int_o^\infty dt\ \psi_n(t)\ \psi_m(t) \qquad (21)$$

and in terms of the Hermite polynomials $H_n(t)$, eq. (21) may be written as

$$S'_{nm} = 2 \int_o^\infty e^{-t^2}\ N_n\ N_m\ H_n(t)\ H_m(t)\ dt\ . \qquad (22)$$

We recall[8] that a product of two Hermite polynomials may be written:

$$H_n(t)\ H_m(t) = \sum_{r\,=\,0}^{\min(n,m)} 2^r\ r!\ \binom{m}{r}\ \binom{n}{r}\ H_{m+n-2r}(t) \qquad (23)$$

so that

$$S'_{nm} = 2 \sum_{r\,=\,0}^{\min(n,m)} 2^r\ r!\ \binom{m}{r}\ \binom{n}{r}\ N_n\ N_m\ H^{(0)}_{m+n-2r-1} \qquad (24)$$

$$S'_{nm} = 2\ N_n\ N_m \sum_{r\,=\,0}^{\min(n,m)} 2^r\ r!\ \binom{m}{r}\ \binom{n}{r}\ (-1)^{\left(\frac{m+n-2r-1}{2}\right)} \times \frac{(m+n-2r-1)!}{\left(\frac{m+n-2r-1}{2}\right)!}$$

or that

$$S'_{nm} = (1 + (-1)^{m+n+1})\ \sqrt{\frac{m!\ n!}{\pi\ 2^{m+n}}}\ (-1)^{\frac{m+n-1}{2}} \times \sum_{r\,=\,0}^{\min(n,m)} \frac{2^r}{r!}\ \frac{(\quad)!\ (\quad)!}{(m-r)!\ (n-r)!}\ \frac{(m+n-2r-1)!}{\left(\frac{m+n-2r-1}{2}\right)!}\ (-1)^r \qquad (25)$$

Equation (18) makes clear that S'_{nm} is a symmetric, real matrix so we may assume $m > n$. We recall that the gamma function ($\Gamma(n+1) = n!$) has the property

$$\Gamma(2z) = \frac{1}{\sqrt{2\pi}}\, 2^{2z-1/2}\, \Gamma(z)\, \Gamma(z+1/2) \quad . \tag{26}$$

The ratio of the factorials involving n + m reduce to

$$\frac{\Gamma(m+n-2r)}{\Gamma\left(\frac{m+n-2r+1}{2}\right)} = \frac{1}{\sqrt{2\pi}}\, 2^{(m+n-2r)-1/2}\, \Gamma\left(\frac{m+n-2r}{2}\right) \tag{27}$$

Let $m = n+2h+1$, then after simplifying, we find

$$S'_{n,\, n+2h+1} = \sqrt{\frac{2\, n!\, (n+2h+1)!}{\pi}}\ (-1)^{n+h} \times \sum_{r=0}^{n} \frac{(-1)^r (2n+2h-2r-1)!!}{r!\, (n+2h-r+1)!\, (n-r)!} \tag{28}$$

The latter relation, although correct in principle to all orders, becomes inaccurate for purposes of compution above n,m ≥35. Therefore, S_{nm} was found from (18) by simply integrating using the zeros of the 500th order Hermite functions as outlined in Appendix A. The latter technique is extremely fast and up to order n+m = 500, is exact

Returning to our original relation (18), we have

$$P(\omega - \omega') = (-i) \sum_{n} \sum_{h} (i)^n\, (-1)^{n+2h+1}\, \psi_n(\omega)\, \psi_{n+2h+1}(\omega') \times S'_{n,\, n+2h+1} \quad . \tag{29}$$

Let us define $S_{n,m}$ such that

$$P(\omega - \omega') = \sum_{nm} S_{nm}\, \psi_n(\omega)\, \psi_m(\omega') \quad . \tag{30}$$

Then the relation between S and S' with m = n+2h+1 is given by

$$S_{nm} = (-1)^{h+1} S'_{nm} \; ; \quad S_{mn} = - S_{nm} \tag{31}$$

The compactness of the operator P can be seen either from equation (4) or from the fact that for fixed n

$$\lim_{h \to \infty} S_{n,\, n+2h+1} \to 0 \tag{32}$$

at least as fast as $(2^{2h}(2h + 1)!!)^{-1}$. The latter is easily proved by direct expansion of equation (28).

We now take up the problem of Hilbert transforms of functions. This problem is especially of interest in exploring the interrelationship of optical properties.

B. Optical Properties

We have seen in the last subsection that the Hermite functions form a compact representation of the Hilbert transform operator. Here we will exploit the fact that these functions also possess simple properties in the complex plane. Two such functions are of practical interest: The complex square root $z^{1/2}$; and the homographic transformation. The first gives the relationship between the dielectric function and the index of refraction; The second the relation between the log of the reflectivity and the index of refraction. Our purpose here is to show that a single set of expansion coefficients of the Hermite functions

characterizes all the optical functions. In particular we will show the inter-relationships between the expansion coefficients.

Let us assume that we have

$$\underset{\sim}{\varepsilon} = \varepsilon_1 + i\varepsilon_2 = \sum_n C_n \psi_n(\omega) \tag{33}$$

and

$$\underset{\sim}{N} = n + ik = \sum_n d_m \psi_n(\omega) \tag{34}$$

where C_n, d_m are complex expansion coefficients which factor into real and wholly imaginary parts as n,m increase (decrease) by 1. Then we have $\underset{\sim}{N} = (\underset{\sim}{\varepsilon})^{1/2}$ or that

$$\begin{aligned} C_m &= \sum_{n\ell} d_n d_\ell \int_{-\infty}^{\infty} d\omega \psi_m(\omega)\ \psi_n(\omega)\ \psi_\ell(\omega) \\ &= \sum_{n\ell} d_n d_\ell\ I^m_{n\ell} \end{aligned} \tag{35}$$

Again exploiting the extremely simple "Clebsh-Gordon" coefficients for the Hermite functions, eq. (23), we have after a little algebra, and assuming that $\ell > n$

$$\begin{aligned} I^m_{n\ell} = N_n\ N_m\ N_\ell \sum_{r=0}^{n} 2^r\ r!\ \binom{n}{r}\ \binom{\ell}{r} \\ \frac{2}{3}\int_{-\infty}^{\infty} H_{n+\ell-2r}\left(\sqrt{\tfrac{2}{3}}\,x\right) H_m\left(\sqrt{\tfrac{2}{3}}\,x\right) e^{-x^2}\,dx \end{aligned} \tag{36}$$

Expanding the latter again using eq. (23) we have

$$I^m_{n\ell} = N_n\, N_m\, N_\ell \sqrt{\frac{2}{3}} \sum_{r=0}^{n} 2^r\, r!\, \binom{n}{r} \binom{\ell}{r}$$

$$\times \frac{1}{\sqrt{\pi}} \sum_{h=0}^{\min(m,\,n+\ell-2r)} 2^h\, h!\, \binom{m}{h} \binom{n+\ell-2r}{h} \left(\frac{1}{3}\right)^{\frac{n+m+\ell-2r-2h}{2}} \tag{37}$$

$$\times H_{n+m+\ell-2r-2h}\,(0)$$

which makes clear that m has the same parity symmetry as $n + \ell$. Let us assume that $n + m + \ell$ is even. Then we have

$$I^m_{n\ell} = N_m\, N_n\, N_\ell \sqrt{\frac{2}{3\pi}} \sum_{r=0}^{n} \sum_{h=0}^{\min(m,\,n+\ell-2r)} 2^{r+h}\, r!\, h!$$

$$\times \binom{n}{r} \binom{\ell}{r} \binom{m}{h} \binom{n+\ell-2r}{h} \left(\frac{1}{3}\right)^{\frac{n+m+\ell-2r-2h}{2}} \tag{38}$$

$$\times (-1)^{\frac{n+m+\ell-2r-2h}{2}} \frac{(n+m+\ell-2r-2h)!}{\left(\frac{n+m+\ell-2r-2h}{2}\right)!}$$

which shows that $I^m_{n\ell}$ is also a compact operator. We stress that the utilization of eq. (38) in practical applications is substantially easier than the form of eq. (38) might initially suggest. We will return to this theme again in Section III.

Finally we consider qualitatively the homographic transformation

$$\underline{Z} = \frac{\alpha\underline{z} - \beta}{\gamma\underline{z} + \delta} \tag{39}$$

and the related transformation

$$\ell n\ \underline{Z} = \ell n(\alpha\underline{z} - \beta) - \ell n(\gamma\underline{z} + \delta) \tag{40}$$

where here $\alpha = \beta = \gamma = \delta = 1$, $\underline{Z}$ is the complex reflectivity $Re^{i\varphi}$ and $\underline{z}$ the complex index of refraction. Since $|\underline{Z}|$, the reflectivity, is bounded by 1, we have that $\ell n(\underline{Z}) = \ell n(1 + (\underline{Z}-1))$ and

$$\log\ (\underline{Z}) = \sum_{n=1}^{\infty} (-1)^n\ \frac{(\underline{Z} - 1)^n}{n + 1} \quad . \tag{41}$$

Exploiting equation (41) on both sides of eq. (40), and by expanding both $\underline{Z}$ and $\underline{z}$ into Hermite functions, and making repeated use of eq. (23), we would come to the conclusion that the operator connecting the two sides of eq. (40) would also be compact. However we believe the analog of equation (38) for the logarithm is too complicated for practical application. We conclude that if a sufficiently great number N were chosen, then an expansion of, for example, any one of the optical functions in the first N Hermite functions with expansion coefficients C_n guarantees that all of the related functions may be found with an error no larger than any given small number ϵ.

III. RESULTS AND APPLICATIONS

Our discussion in the last section was purely formal and essentially hinged on showing the compactness of various operators, in terms of Hermite functions. Here we will be entirely concerned with the practical application of our formal results to real systems. We will also slightly extend our definition of expansion and furthermore show compactness in the important case of finite data ranges.

A. s-band Density of States

First we consider a problem in which the function to be transformed is defined everywhere. We apply our results to the important problem of deriving the "F" function for the density of states of s states in the simple cubic lattice:

$$F(\omega) = \frac{P}{\pi} \int_{-\infty}^{\infty} d\omega' \ \frac{g(\omega')}{\omega' - \omega} \tag{42}$$

where

$$g(\omega') = \frac{2}{(2\pi)^3} \int d\underline{h}\, \delta\,(E\,(\underline{h}) - \omega') \quad , \tag{43}$$

$$E\,(\underline{h}) = \cos\,(h_x a) + \cos\,(h_y a) + \cos\,(h_z a) \quad , \tag{44}$$

and $-\frac{\pi}{a} < h_x, h_y, h_z < \frac{\pi}{a}$. In Figure 1(a) we plot a three hundred histogram approximation to (43), where we have used

one-million Monte Carlo points[9] to integrate (43). We notice that whereas (43) is completely a symmetric function around $\omega' = 0$, our Monte Carlo approximation has a small, but finite, odd part. Normally this imperfection should be removed by symmetrizing, but here this is not necessary since our operator form of the Hilbert kernel, eq. (30), does not depend on the parity of the expansion functions except in that even functions are transformed into odd ones, etc. Moreover the small odd part of $g(\omega)$ forms a measure of the error in the Monte Carlo integration. By expanding the delta function, we may write (43) as

$$g(\omega) = \frac{2}{2\pi} \int_{-\infty}^{\infty} dt \cos \omega t \, J^3{}_0(t) \quad , \tag{45}$$

a form first utilized by Callaway.[10]

The Hilbert transform of $g(\omega)$ is

$$F(w) = \frac{P}{\pi} \int \frac{dw'}{w-w'} g(w') \ .$$

Thus we have the analytic representations:

$$\begin{Bmatrix} g(w) \\ F(w) \end{Bmatrix} = \frac{2}{\pi} \int_0^{\infty} dt \, J_0^3(t) \begin{Bmatrix} \cos(wt) \\ \sin(wt) \end{Bmatrix} \ .$$

Figure 1 gives the result of integrating the above forms at the 250 positive zeros of the 500th order Hermite function by Hermite integration (see Appendix A).

Although the Hermite expansions are exact in principle, the convergence of the expansion in Hermite functions may be substantially improved by removing the low order moments from $g(w)$ and transforming these analytically. Then a Laurent expansion of $F(w)$ will begin with order

m+1 as

$$\frac{P}{w-w'} = \frac{P}{w} \sum_{m=0}^{\infty} \left(\frac{w'}{w}\right)^m ,$$

so that

$$F(w) = \frac{1}{\pi} \frac{P}{w} \sum_{m=0}^{\infty} w^{-m} \int_{-\infty}^{+\infty} dw' \; w'^m g(w).$$

In practice good results are achieved if only the zeroth moment is removed. From g(w) the triangle-like function $g_s(w)$ is subtracted where

$$g_s(w) = \frac{2}{3}\left[1 - SGN(w)w/3\right].$$

This function is also plotted in Fig. 1 ($\int g_s(w)dw = 2$). The analytic transform of this is given by

$$F_s(w) = -\frac{2}{3\pi}\left[\ell n \left|\frac{w-3}{w+3}\right| - \frac{w}{3} \ell n \left|\frac{(w-3)(w+3)}{w^2}\right|\right]$$

This is also plotted in Fig. 1. Note that to first order, the log poles are subtracted out. The residium of has been expanded using the first 250 Hermite functions and a scale factor of $\alpha = 6\sqrt{2N+1}$ where N = 250 so that, in effect, the highest functions just span the range from 0 to 6. This scaling avoids any "edge effects" due to a confluence of the upper level of the range of integration and the Hermite function expansion set. Table I lists the first 20 expansion coefficients.

Since Fig. 1 plots both $g(\omega)$ and $F(\omega)$ on the same scale, we see that the four critical points of $g(\omega)$ are mapped into four points at the same ω, except that the types[11] of critical points have interchanged under Hilbert transform; i.e., $M_0 \quad M_1 \quad M_3$. We conclude from this example that critical point structure cannot shift under a proper Hilbert transformation.

B. Transition Metal

For our second example we consider the electronic structure of a face centered cubic pure transition metal--here palladium as calculated by Mueller, Freeman, Dimmock and Furdyna.[12] We recall that the non-interacting electronic Greens' function in the momentum and frequency representation for n bands is given by[13]

$$G^0(\underline{k},\omega) = \sum_n (\omega - E_n(\underline{k}) + i\delta \, \mathrm{SGN} \, (E_n(\underline{k}) - \mu))^{-1} \qquad (48)$$

where δ is an infinitesimal and μ is the Fermi energy E_F. The imaginary part of (48) is given by

$$I_m\, G^o(\underline{k},\omega) = -\pi \sum_n SGN(E_n(\underline{k}) - \mu)\ \delta\ (E_n(\underline{k}) - \omega) \qquad (49)$$

and the density of states by:

$$g(\omega) = \frac{-1}{\pi}\ SGN\ (\omega-\mu)\ \frac{2}{(2\pi)^3} \int I_m\, G^o(\underline{k},\omega)\ d\underline{k} \quad . \qquad (50)$$

In Figure 3(a) we have plotted the weighted integral over the Brillouin zone (BZ) of the imaginary part of $G^o(\underline{k},\omega)$. The dispersion relation for the Greens' function is given by:

$$Re\ G(\underline{k},\omega) = \frac{P}{\pi} \int_{-\infty}^{\infty} d\omega'\ \frac{I_m G(\underline{k},\omega') SGN(\omega'-\mu)}{\omega' - \omega} \qquad (51)$$

where the presence of signum function in (51) removes the signum function in (49), so that the integral to be performed in (51) is just the principal part of a delta function. Here we consider only the ω dependence of (51) by integrating (51) over the first BZ to produce the Hilbert transform pair $\underline{G} = G_R + iG_I$ where

$$G_R(\omega) = \frac{2}{(2\pi)^3} \int Re\ G(\underline{k},\omega)\ d\underline{k} \quad . \qquad (52)$$

and

$$G_I(\omega) = \pi\, g\ (\omega) \quad . \qquad (53)$$

We have taken the Hilbert transform of (53) using the method given in Section II by expanding $wf(\omega)$ in the first three-hundred Hermite functions. We have used a scale factor α = 24.51 found from TOP* $\alpha = (2^*N + 1)^{1/2}$ where here TOP = 1 and N = 600. We

notice that the fact that $g(\omega)$ has no parity symmetry does not harm our completely general transformation, eq. (30). We give our results in Figure 3(b), and again list the first 20 expansion coefficients in Table II. Note that we have used atomic units of states per atom-Rydberg for both the real and imaginary parts. The total time for our routines for the 300 term expansion was 10 minutes on the IBM 360/50/75 at the Applied Mathematics Division at Argonne National Laboratory.

IV. Summary and Discussion

In this paper we have considered an exact numerical procedure for finding the Kramers-Kronig or Hilbert transform of a given function by means of an expansion in terms of Hermite functions. Although our procedure is most easily applied to cases where the function to be transformed is defined over the whole, real line, we have seen that simple extensions of the notion of least-square fitting allow us to treat the practically important case of a function defined only over a region. We have seen that the compactness of our expansion allows us to treat the special case of optical data, which has several variables related by non-linear equations, by means of a single set of expansion coefficients of the Hermite functions. We have stressed that although our procedures are well-defined in the case of evenly spaced data, the best use of our techniques will be achieved if the data is spaced by the zeros of a high order Hermite polynomial. We believe that

the advantages of the latter procedure are so great that all optical experiments should be performed in this way.

Because of the simplicity and speed of expansion of numerical functions in terms of Hermite polynomials, we believe that our procedures should prove useful in a wide variety of problems. Moreover we stress that because the Hilbert transform has been performed analytically, rather than numerically, our results are independent of the "noise" or discontinuities of the data. We believe that this is not true of numerical procedures which operate on data directly. Finally although all of our discussion of this paper has been couched in terms of the Hilbert transform, we point out that our procedures are equally valid for the Fourier transform operator, eq. (15). Thus in contrast to Russel[17] who concluded in 1933 that "this use of Hermite functions (i.e., Fourier transformation) ... is, in general, not practicable," we believe that Hermite functions are eminently suitable for such numerical work. Only future results can determine whether such an expansion technique in Hermite function would be actually faster than "The Fast Fourier Transform Method[18]."

V. ACKNOWLEDGMENTS

We wish to thank Professor C. Wood of for stimulating our interest in this problem.

and for helpful discussions. We would also like to thank Drs. B. Veal, J. E. Robinson, J. W. Garland and S. Kirkpatrick and N. Dolton for useful conversations. Finally we wish to acknowledge W. J. Cody of the Applied Mathematics Division of Argonne National Laboratory for helpful consultations on the Hermite function generator programs.

APPENDIX A HERMITE INTEGRATION

Here we consider Hermite integration of a function defined over the whole real line. A thorough discussion of this problem has been given by Hochstrasser[19] and Davis and Polansky[20] based on the classic work of Russel[21] and Salzer[22] et.al. Our results differ from that of the previous workers only in that we have gone to higher order 23 and used a different weight function. Hermite integration of a function f(x) to order n is given by

$$\int_{-\infty}^{\infty} e^{-x^2} f(x)\, dx = \sum_{i=1}^{n} W_n(x_i^n)\, f(x_i^n) \qquad (A1)$$

where x_i^n is the ith zero of the nth order Hermite polynomial H_n, and the weight factors W_n are given by

$$W_n(x_i^n) = \frac{2^{n-1}\, n!\, \sqrt{\pi}}{n^2\, [H_{n-1}(x_i^n)]^2} \qquad (A2)$$

A numerically more convenient representation for Hermite integration is achieved if we consider instead

$$\int_{-\infty}^{\infty} g(x)\, dx = \sum_{i=1}^{n} W'_n(x_i^n)\, g(x_i^n) \qquad (A3)$$

where W_n' is given by

$$W'_n(x_i^n) = W_n(x_i^n) \exp(x_i^{n^2}) = 1/(n\psi_{n-1}^2(x_i^n)) \qquad (A4)$$

where ψ_n is the n'th order orthonormal Hermite function. In Table IV we list the positive zeros and weight functions W_n' for the Hermite polynomials of order 20, 26, 50, 76, 150 and 300. For the overlapping case of n = 20, over results agree with those of Salzer, et al. to at least 14 significant figures.

We have found the zeros of the Hermite polynomials (or Hermite functions) by noticing that the sequence of polynomials H_o, H_1 ... H_n form a Sturm sequence. Thus by counting the number of sign changes in the sequence, we know precisely, by Budan's Theorem, the number of zeros between a given point x and zero. (Infinitesimally above zero the sign of all the Hermite polynomials is plus). An estimate of the largest zero of the Hermite polynomial of order n is found by remembering that the Hermite functions are eigenfunctions (with eigenvalue $E_n = (n+1/2)\hbar\omega$) of the simple harmonic oscillator operator, $H = \frac{p^2}{2m} + \frac{1}{2}k\,x^2$, where $\omega = \sqrt{\frac{k}{m}}$. We recall that the probability density of the nth harmonic oscillator eigenfunction is bounded by the classical

limit, $\sqrt{\frac{2E_n}{k}}$, or in the appropriate units (m = k = 1), by $x_{max} = \sqrt{2n + 1}$. Thus all of the zeros of the n'th Hermite polynomial lie between $\pm \sqrt{2n + 1}$.

Our computational procedure for evaluating the zeros of the n'th polynomial used the interval given by the absolute bounds $\pm\sqrt{2n + 1}$ and continuously sub-divided this interval by a factor of 2. Each subinterval was selected for further operation depending on whether the Sturm sequence predicted an appropriate zero in the left or right-hand portions. Such a procedure quickly, and accurately converged to our results in Table IV. We have tested our zeros through the sum rule:

$$\sum_{i=1}^{n} (x_i^n)^2 = \frac{n\,(n - 1)}{2} \qquad (A5)$$

to an accuracy of at least 14 significant figures.

REFERENCES

[1]R. Kronig, J. Opt. Soc. Amer. 12, 547 (1926).

[2]H. A. Kramers, Atti Congr. Intern. Fisici, Como, 2, 545 (1927).

[3]E. C. Titchmarsh, Introduction to the Theory of Fourier Integrals (Claredon Press, Oxford, 1948).

[4]M. J. Lighthill, Introduction to Fourier Analysis and Generalized Functions, (University Press, Cambridge, 1959).

[5]N. Dunford and J. T. Schwartz, Linear Operators Part II: Spectral Theory, (Interscience Publishers, New York London, 1963) Section XI.7.

[6]See, for example, D. Pines, Elementary Excitations in Solids, (W. A. Benjamin, Inc., New York Amsterdam, 1963), pp. 288.

[7]E. C. Titchmarsh, ibid., pp. 76.

[8]W. Magnus, F. Oberhettinger, R. Pal Soni, Die Grundlehren der Mathematischen Wissenshaften, Band 52, (Springer-Verlag, Inc., New York, 1966) pp. 249. Note that the definition of the third Hermite polynomial, $H_3(x)$, on page 250 is incorrect. The correct result is $H_3(x) = 8x^3 - 12x$.

[9]This point is discussed thoroughly in F. M. Mueller, J. W. Garland, M. H. Cohen, and K. H. Bennemann, (to be published).

[10]J. Callaway and A. J. Hughes Phys. Rev. 128, 134 (1962).

[11]J. C. Phillips, Phys. Rev. 104, 1263 (1956).

[12]F. M. Mueller, A. J. Freeman, J. O. Dimmock , and A. M. Furdyna, Phys. Rev. (in press).

[13]A. A. Abrikosov, L. P. Gorkov, and I. Ye. Dzyaloshinshii, Quantum Field Theoretical Methods in Statistical Physics, second edition, translated by D. E. Brown, (Pergamon Press, Oxford, 1965) pp. 51.

[14]See, for example, C. Lanczos, Applied Analysis, (Prentice Hall, Inc., New Jersey, 1956).

[15]Lanczos, ibid., Chapter II.

[16]C. Wood (to be published).

[17]J. B. Russel, Journal of Mathematics and Physics, 12, 274 (1933).

[18]J. W. Cooly and J. W. Tukey, Math of Computer 19, 297 (1965), R. Klahn and R. R. Shivley, Electronics 41, 124 (1968), M. L. Forman, J. Opt. Soc. Am. 56, 978 (1966).

[19]V. W. Hochstrasser, Handbook of Mathematical Functions, ed. by M. Abramowitz and I. A. Stegun, (Dover Publications, Inc., New York, 1965), Chapter 22.

[20]P. J. Davis and I. Polarsky, op. cit., Chapter 25.

[21]J. B. Russel, Journal of Mathematics and Physics 12, 291 (1933).

[22]H. E. Salzer, R. Zuker, and R. Capuaro, J. Research NBS 48, 111 (1952).

[23]See also A. H. Stroud and D. Seirest, Gaussian Quadrative Formulas, (Prentice-Hall, Inc., New Jersey, 1966) for 0 to 136, even to 30 decimal places where the weight factor (A2) is used.

[24]C. H. Page, Physical Mathematics (van Nostrand, New York, 1955), p. 237.

[25]Copies of these programs, as well as the punched cards for the zeros are available on request. We believe that because of the simple error spectrum in generating Hermite functions (only rounding errors), that our numerical procedures are accurate to arbitrarily high order. Cost is the only limiting factor.

TABLE I The first few Hermite function expansion coefficients of the triple cosine density of states. As explained in the text, the scale factor $\alpha = 6/\sqrt{2N+1}$ was used where here N = 150. The coefficient for C_n (D_n) are non-zero for even (odd) order because they were derived from a Monte-Carlo function which was accurate to about 1%. Note that the convergence of D is much slower than C. Removing the zeroth moment from g(w), as explained in the text, greatly improves this rate so that the expansion of the residual of D is essentially zero after N = 75.

n	C_n		D_n
0	1.0758		0.0010
1	-0.0019		0.2436
2	0.7517		-0.0008
3	-0.0009		0.3469
4	0.6029		0.0002
5	-0.0042		0.4376
6	0.4306		-0.0053
7	0.0007		0.4434
8	0.2842		-0.0045
9	0.0037		0.3696
10	0.2355		-0.0015
20	0.1263	(n+1)	0.2815
40	0.0048		0.1926
60	0.0054		0.1232
80	-0.0002		0.0977
100	0.0001		0.0796
120	0.0008		0.0730
140	-0.0005		0.0693

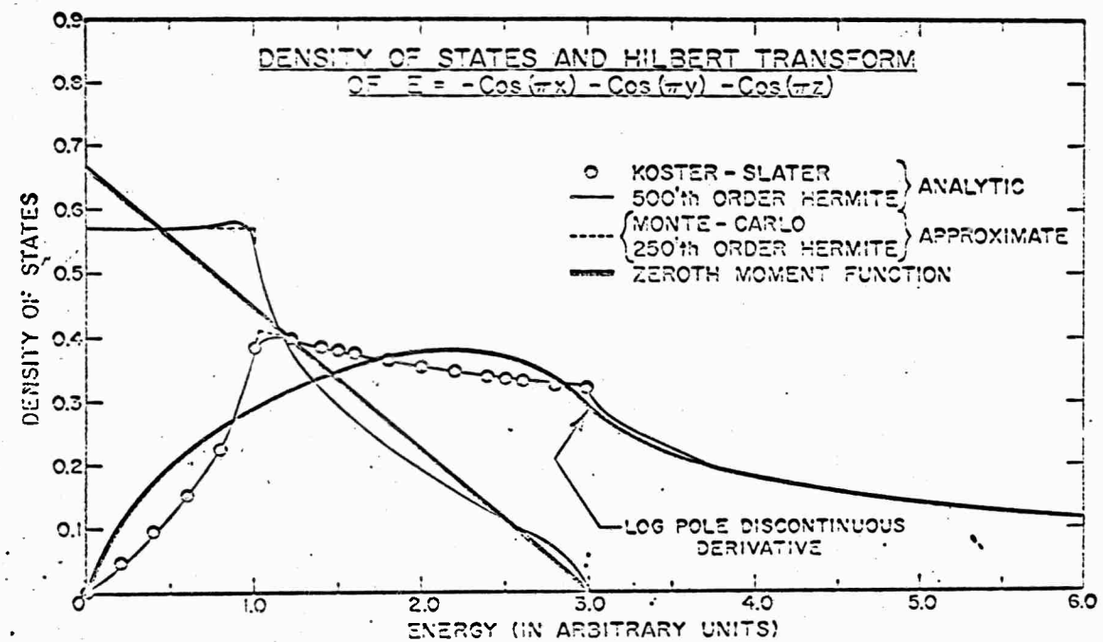

Fig. 1. The density of states and Hilbert transform of the triple cosine density of states.

TABLE IV. The Positive Zeros and Weight Functions for Hermite Integration for Various High Orders. Note that the brackets at the end of each number enclose a multiplicative power of 10.

i	N = 20 X_i^n	$W_n'(X_i^n)$
1	0.245340708300901(00)	0.490921500666746(00)
2	0.737473728545394(00)	0.493843385272053(00)
3	0.123407621539532(01)	0.499920871336291(00)
4	0.173853771211659(01)	0.509679027117459(00)
5	0.225497400208928(01)	0.524080350948559(00)
6	0.278880605842813(01)	0.544851742364521(00)
7	0.334785456738322(01)	0.575262442852505(00)
8	0.394476404011563(01)	0.622278696191415(00)
9	0.460368244955074(01)	0.704332961176944(00)
10	0.538748089001123(01)	0.898591961453191(00)

i	N = 26 X_i^n	$W_n'(X_i^n)$
1	0.215777856243463(00)	0.431682072931449(00)
2	0.648095213993448(00)	0.433211201157933(00)
3	0.108273301107788(01)	0.436341269581532(00)
4	0.152136151665192(01)	0.441226060840462(00)
5	0.196585478564114(01)	0.448124652400575(00)
6	0.241841576477378(01)	0.457445500520743(00)
7	0.288176221954309(01)	0.469827981244890(00)
8	0.335942718235083(01)	0.486299148276451(00)
9	0.385628841990915(01)	0.508598868349973(00)
10	0.437960266298331(01)	0.539935445971070(00)
11	0.494132495724138(01)	0.587063315389790(00)
12	0.556452498195010(01)	0.667757331454302(00)
13	0.630955038562569(01)	0.856242029971326(00)

i	N = 50 X_i^n	$W_n'(X_i^n)$
1	0.156302540[illegible](00)	0.312630298030360(00)
2	0.469059[illegible](00)	0.312933442052390(00)
3	0.782271[illegible](00)	0.313543599[illegible]642(00)
4	0.109629[illegible](01)	0.314[illegible]2473(00)
5	0.141131[illegible](01)	0.315720440230094(00)

i	N = 50 X_i^n	$W_n'(X_i^n)$
6	0.172780654751590(01)	0.317316124349605(00)
7	0.204607196868641(01)	0.319277915993182(00)
8	0.236649390429866(01)	0.321624537962057(00)
9	0.268948470226775(01)	0.324422448708867(00)
10	0.301549776957452(01)	0.327687661354607(00)
11	0.334503831393789(01)	0.331488254247523(00)
12	0.367867706251527(01)	0.335897876837687(00)
13	0.401706817285813(01)	0.341010727258748(00)
14	0.436097316045458(01)	0.346948769599379(00)
15	0.471129366616904(01)	0.353872469979462(00)
16	0.506911758491724(01)	0.361997265091619(00)
17	0.543578608722495(01)	0.371619771249917(00)
18	0.581299467542041(01)	0.383161392196480(00)
19	0.620295251927467(01)	0.397244943775848(00)
20	0.660864797385536(01)	0.414838821059023(00)
21	0.703432350977061(01)	0.437553282300050(00)
22	0.748640942986420(01)	0.468326211942548(00)
23	0.797562236820564(01)	0.513304797851543(00)
24	0.852277103091780(01)	0.588605297377302(00)
25	0.918240695812932(01)	0.761348691118096(00)

i	N = 76 X_i^n	$W_n'(X_i^n)$
1	0.126992231001841(00)	0.253993385676772(00)
2	0.381030264410276(00)	0.254100577463541(00)
3	0.635229306367669(00)	0.254315550492752(00)
4	0.889697681755121(00)	0.254639493166670(00)
5	0.114454521094402(01)	0.255074212122994(00)
6	0.139888384198577(01)	0.255622161952324(00)
7	0.165582831812922(01)	0.256286486333430(00)
8	0.191249689274787(01)	0.257071071989737(00)
9	0.217001210540204(01)	0.257980617366250(00)
10	0.242850163495476(01)	0.259020718536551(00)
11	0.268809924853835(01)	0.260197975618256(00)
12	0.294894536891950(01)	0.261520123961741(00)
13	0.321119078708898(01)	0.262996195662676(00)
14	0.347499305806231(01)	0.264636718648907(00)
15	0.374052310941034(01)	0.266453962869778(00)
16	0.400790463063241(01)	0.268462246207442(00)
17	0.427751683211511(01)	0.270678316981588(00)
18	0.454939704768905(01)	0.273121835247604(00)
19	0.482354405 [illegible]	0.275815 [illegible] 275816(00)
20	0.510112105 [illegible]	0.27 [illegible] 270852212(00)

i	N = 76 x_i^n	$W_n'(x_i^n)$
21	0.5381524121798 50(01)	0.282071512255670(00)
22	0.5665381427504 30(01)	0.285705215988960(00)
23	0.5953067244596 81(01)	0.289737351776540(00)
24	0.6245008406791 73(01)	0.294226784433783(00)
25	0.6541697408802 43(01)	0.299246627607381(00)
26	0.6843708879718 93(01)	0.304888971325212(00)
27	0.7151721755950 64(01)	0.311271705500812(00)
28	0.7466549797883 78(01)	0.318548640662417(00)
29	0.7789184688388 88(01)	0.326925003272138(00)
30	0.8120858775452 08(01)	0.336682064992593(00)
31	0.8463139782058 18(01)	0.348218086208989(00)
32	0.8818080214626 19(01)	0.362120212339010(00)
33	0.9188466371460 59(01)	0.379299672898844(00)
34	0.9578263684375 55(01)	0.401269503496751(00)
35	0.9993491992840 45(01)	0.430787054460799(00)
36	0.1044419184013 67(01)	0.473616168889675(00)
37	0.1094986156437 31(02)	0.544854576829319(00)
38	0.1156159236754 24(02)	0.707324524548646(00)

i	N = 100 x_i^n	$W_n'(x_i^n)$
1	0.1107958724224 40(00)	0.221596255924184(00)
2	0.3324146923422 32(00)	0.221650420411516(00)
3	0.5541148235916 17(00)	0.221758921729024(00)
4	0.7759507415401 46(00)	0.221922106165498(00)
5	0.9979774360981 05(00)	0.222140497191774(00)
6	0.1220250391218 95(01)	0.222414800390545(00)
7	0.1442825970215 93(01)	0.222745910173358(00)
8	0.1665761509741 51(01)	0.223134918413969(00)
9	0.1889115537427 01(01)	0.223583125167178(00)
10	0.2112947996371 19(01)	0.224092051687791(00)
11	0.2337320463906 88(01)	0.224663456017246(00)
12	0.2562290402372 61(01)	0.225299351467709(00)
13	0.2787941423981 99(01)	0.226002028407800(00)
14	0.3014323580331 16(01)	0.226774079843686(00)
15	0.3241513679631 01(01)	0.227618431398403(00)
16	0.3469585636411 59(01)	0.228538376426247(00)
17	0.3698616859311 49(01)	0.229537617164871(00)
18	0.3928688683427 67(01)	0.230620313034513(00)
19	0.4159883955131 03(01)	0.231791137453704(00)
20	0.4392302079686 23(01)	0.233056344869711(00)
21	0.4626 [illegible] (01)	0.234 [illegible] (00)
22	0.4861175091791 21(01)	0.235 [illegible] (00)

i	N = 100 X_i^n	$W_n'(X_i^n)$
23	0.509784510508914(01)	0.237471299920463(00)
24	0.533615836013836(01)	0.239176321299560(00)
25	0.557624164932992(01)	0.241013092922388(00)
26	0.581823213520352(01)	0.242992685579109(00)
27	0.606227883261430(01)	0.245127777913569(00)
28	0.630854436111214(01)	0.247432956126835(00)
29	0.655720703192154(01)	0.249925086601289(00)
30	0.680846335285880(01)	0.252623783391418(00)
31	0.706253106024887(01)	0.255552000562022(00)
32	0.731965282230454(01)	0.258736790904382(00)
33	0.758010080785749(01)	0.262210289443759(00)
34	0.784418238446082(01)	0.266011005285956(00)
35	0.811224731116279(01)	0.270185543533994(00)
36	0.838469694041626(01)	0.274790938326840(00)
37	0.866199616813452(01)	0.279897872545095(00)
38	0.894468921732547(01)	0.285595214531379(00)
39	0.923342089021916(01)	0.291996563960282(00)
40	0.952896582339012(01)	0.299249958039083(00)
41	0.983226980777797(01)	0.307552728501676(00)
42	0.101445099412928(02)	0.317175110971854(00)
43	0.104671854213428(02)	0.328499484645464(00)
44	0.108022607536847(02)	0.342089262314264(00)
45	0.111524043855851(02)	0.358818409071116(00)
46	0.115214154007870(02)	0.380137438800590(00)
47	0.119150619431142(02)	0.408688658441919(00)
48	0.123429642228597(02)	0.449993171054426(00)
49	0.128237997494878(02)	0.518506807270215(00)
50	0.134064873381449(02)	0.674353552420927(00)

i	N = 150 X_i^n	$W_n'(X_i^n)$
1	0.905393562173930(01)	0.181080356250504(00)
2	0.271627932943462(00)	0.181100087161783(00)
3	0.452746116521430(00)	0.181139576950067(00)
4	0.633913691503[illegible](00)	0.181198881662550(00)
5	0.815150512623287(00)	0.181278085660326(00)
6	0.996476533271402(00)	0.181377301969454(00)
7	0.117791[illegible](01)	0.181496672753586(00)
8	0.135947665389839(01)	0.181636369912105(00)
9	0.154119141677934(01)	0.181796595808372(00)
10	0.172307677096772(01)	0.[illegible](00)
11	0.190515[illegible](01)	0.[illegible](00)
12	0.208744307[illegible](01)	0.[illegible](00)

i	N = 150 X_i^n	$W_n'(X_i^n)$
13	0.226996670601846(01)	0.182647952897092(00)
14	0.245274632650825(01)	0.182914993130992(00)
15	0.263580417243331(01)	0.183204475153263(00)
16	0.281916290649120(01)	0.183516847605137(00)
17	0.300284566085444(01)	0.183852601168485(00)
18	0.318687608037202(01)	0.184212270930110(00)
19	0.337127836826775(01)	0.184596439015283(00)
20	0.355607733461688(01)	0.185005737515972(00)
21	0.374129844791178(01)	0.185440851745961(00)
22	0.392696789006054(01)	0.185902523858022(00)
23	0.411311261520057(01)	0.186391556863946(00)
24	0.429976041275279(01)	0.186908819104070(00)
25	0.448693997519212(01)	0.187455249219867(00)
26	0.467468097106740(01)	0.188031861691191(00)
27	0.486301412387000(01)	0.188639753009181(00)
28	0.505197129742681(01)	0.189280108566815(00)
29	0.524158558858165(01)	0.189954210362072(00)
30	0.543189142803131(01)	0.190663445623924(00)
31	0.562292469030160(01)	0.191409316489508(00)
32	0.581472281398769(01)	0.192193450882319(00)
33	0.600732493354504(01)	0.193017614766968(00)
34	0.620077202410791(01)	0.193883725986847(00)
35	0.639510706103660(01)	0.194793869927954(00)
36	0.659037519615962(01)	0.195750317297001(00)
37	0.678662395299107(01)	0.196755544356059(00)
38	0.698390344357807(01)	0.197812256022201(00)
39	0.718226661008041(01)	0.198923412321662(00)
40	0.738176949472241(01)	0.200092258787764(00)
41	0.758247154240578(01)	0.201322361515414(00)
42	0.778443594105884(01)	0.202617647738750(00)
43	0.798773000575715(01)	0.203982452991046(00)
44	0.819242561382582(01)	0.205421576148721(00)
45	0.839859969958369(01)	0.206940343969012(00)
46	0.860633481918744(01)	0.208544687124325(00)
47	0.881571979827913(01)	0.210241230242131(00)
48	0.902685047796305(01)	0.212037399116090(00)
49	0.923983057821401(01)	0.213941549112823(00)
50	0.945477270238304(01)	0.215963119932604(00)
51	0.967179951234435(01)	0.218112823393272(00)
52	0.989104511146228(01)	0.220402872941481(00)
53	0.101126566825741(02)	0.222847266365845(00)
54	0.103367964414043(02)	0.225462137004520(00)
55	0.105636439841120(02)	0.228266194068376(00)
56	0.107933991301043(02)	0.231281280245528(00)
57	0.110262853903433(02)	0.234533095595758(00)
58	0.112625542055057(02)	0.238052072592405(00)
59	0.115024906701541(02)	0.241874690760717(00)

i	N = 150 x_i^n	$W_n'(x_i^n)$
60	0.117464194650572(02)	0.2460449951973340(00)
61	0.119947143660916(02)	0.2506168389216390(00)
62	0.122478090271675(02)	0.2556568976696900(00)
63	0.125062118986053(02)	0.2612489309684600(00)
64	0.127705261907239(02)	0.2674999288882700(00)
65	0.130414773515685(02)	0.2745492244019660(00)
66	0.133199518700414(02)	0.2825824383112990(00)
67	0.136070537533689(02)	0.2918536342897300(00)
68	0.139041897535625(02)	0.3027221330636210(00)
69	0.142132037639839(02)	0.3151712910954000(00)
70	0.145366007090890(02)	0.3316591458812180(00)
71	0.148779467631425(02)	0.3519094094386660(00)
72	0.152426555099726(02)	0.3789464922165930(00)
73	0.156397529899877(02)	0.4179470309538150(00)
74	0.160867551059297(02)	0.4824584152956720(00)
75	0.166295094788339(02)	0.6287963299619510(00)

i	N = 300 X_i^n	$W_n'(X_i^n)$
1	0.640741472402192(01)	0.128148586278527(00)
2	0.192224192571379(00)	0.128152088083630(00)
3	0.320379491076731(00)	0.128159092938003(00)
4	0.448543546946482(00)	0.128169603331269(00)
5	0.576719867484211(00)	0.128183623001091(00)
6	0.704911964356741(00)	0.128201156937050(00)
7	0.833123354848544(00)	0.128222211385832(00)
8	0.961357563121985(00)	0.128246793857734(00)
9	0.108961812148474(01)	0.128274913134490(00)
10	0.121790857166569(01)	0.128306579278457(00)
11	0.134623246610075(01)	0.128341803643157(00)
12	0.147459336922983(01)	0.128380598885211(00)
13	0.160299485880652(01)	0.128422978977690(00)
14	0.173144052722181(01)	0.128468959224895(00)
15	0.185993398284332(01)	0.128518556278625(00)
16	0.198847885137154(01)	0.128571788155945(00)
17	0.211707877721467(01)	0.128628674258499(00)
18	0.224573742488346(01)	0.128689235393416(00)
19	0.237445848040787(01)	0.128753493795845(00)
20	0.250324565277703(01)	0.128821473153176(00)
21	0.263210267540432(01)	0.128893198630997(00)
22	0.276103330761931(01)	0.128968696900846(00)
23	0.289004133618831(01)	0.129047996169817(00)
24	0.301913057686559(01)	0.129131126212093(00)
25	0.314830487597702(01)	0.129218118402481(00)
26	0.327756811203834(01)	0.129309005752003(00)
27	0.340692419741004(01)	0.129403822945667(00)
28	0.353637707991?0(01)	0.129502606382463(00)
29	0.366593074495444(01)	0.129605394217719(00)
30	0.379558921652440(01)	0.129712226407881(00)
31	0.392535655980238(01)	0.129823144757859(00)
32	0.405523688263951(01)	0.129938192971039(00)
33	0.418523433756145(01)	0.130057416702080(00)
34	0.431535312374723(01)	0.130180863612652(00)
35	0.444559748906545(01)	0.130308583430233(00)
36	0.457597173217077(01)	0.130440628010123(00)
37	0.470648020466418(01)	0.130577051400859(00)
38	0.483712731332040(01)	0.130717909913169(00)
39	0.496791752238613(01)	0.130863262192688(00)
40	0.509885535595289(01)	0.131013169296599(00)
41	0.522994540040867(01)	0.131167694774446(00)
42	0.536119230697249(01)	0.131326904753321(00)
43	0.549260079431646(01)	0.131490868027683(00)
44	0.562417565128007(01)	0.131659656154062(00)
45	0.575592173968179(01)	0.131833343550936(00)
46	0.588784399723317(01)	0.132012007040?1(00)
47	0.601994744056127(01)	0.132195723777664(00)

N = 300

i	x_1^n	$W_n'(x_1^n)$
48	0.615223716834511(01)	0.132384590731631(00)
49	0.628471836457277(01)	0.132578680335272(00)
50	0.641739630192552(01)	0.132778088348087(00)
51	0.655027634529639(01)	0.132982908457699(00)
52	0.668336395545051(01)	0.133193238525665(00)
53	0.681666469283536(01)	0.133409180191540(00)
54	0.695018422154947(01)	0.133630839145774(00)
55	0.708392831347863(01)	0.133858325301981(00)
56	0.721790285260936(01)	0.134091752979220(00)
57	0.735211383952988(01)	0.134331241094941(00)
58	0.748656739612971(01)	0.134576913369326(00)
59	0.762126977050959(01)	0.134828895541787(00)
60	0.775622734211436(01)	0.135087330600484(00)
61	0.789144662710220(01)	0.135352349025737(00)
62	0.802693428396470(01)	0.135624099048361(00)
63	0.816269711941308(01)	0.135902731923935(00)
64	0.829874209454720(01)	0.136188405224215(00)
65	0.843507633132506(01)	0.136481283146922(00)
66	0.857170711935176(01)	0.136781536845252(00)
67	0.870864192300860(01)	0.137089344778620(00)
68	0.884588838894404(01)	0.137404893086255(00)
69	0.898345435395049(01)	0.137728375985364(00)
70	0.912134785325241(01)	0.138059996195847(00)
71	0.925957712923309(01)	0.138399965393597(00)
72	0.939815064063013(01)	0.138748504694727(00)
73	0.953707707223158(01)	0.139105845173204(00)
74	0.967636534510753(01)	0.139472228414639(00)
75	0.981602462741485(01)	0.139847907109224(00)
76	0.995606434581581(01)	0.140233145687203(00)
77	0.100964941975549(02)	0.140628221000407(00)
78	0.102373241632419(02)	0.141033423053899(00)
79	0.103785645203934(02)	0.141449055792188(00)
80	0.105202258577901(02)	0.141875437944763(00)
81	0.106623190907108(02)	0.142312903936427(00)
82	0.108048554771127(02)	0.142761804868347(00)
83	0.109478466348299(02)	0.143222509576357(00)
84	0.110913045598719(02)	0.143695405773886(00)
85	0.112352416459115(02)	0.144180901287641(00)
86	0.113796707050575(02)	0.144679425395006(00)
87	0.115246049900201(02)	0.145191430273312(00)
88	0.116700582177869(02)	0.145717392572203(00)
89	0.118160445949367(02)	0.146257815121696(00)
90	0.119625788447361(02)	0.146813228789954(00)
91	0.121096762361745(02)	0.147384194506735(00)
92	0.122573526151134(02)	0.147971305470132(00)
93	0.124056244377416(02)	0.148575169556806(00)

N = 300

i	x_i^n	$W_n'(x_i^n)$
94	0.125545088065523(02)	0.149196511958192(00)
95	0.127040235090794(02)	0.149835978068364(00)
96	0.128541870596601(02)	0.150494336652432(00)
97	0.130050187445190(02)	0.151172383328534(00)
98	0.131565386705064(02)	0.151870964400786(00)
99	0.133087678178635(02)	0.152590981086028(00)
100	0.134617280974304(02)	0.153333394183268(00)
101	0.136154424127682(02)	0.154099229241913(00)
102	0.137699347277255(02)	0.154889582993313(00)
103	0.139252301400482(02)	0.155705626219885(00)
104	0.140813549617129(02)	0.156548617847856(00)
105	0.142383368067554(02)	0.157419905863159(00)
106	0.143962046874742(02)	0.158320939666510(00)
107	0.145549891200145(02)	0.159253279302607(00)
108	0.147147222404828(02)	0.160218606621943(00)
109	0.148754379329162(02)	0.161218737860854(00)
110	0.150371719706303(02)	0.162255637859000(00)
111	0.151999621727093(02)	0.163331436173422(00)
112	0.153638485776849(02)	0.164448445397047(00)
113	0.155288736367860(02)	0.165609182049064(00)
114	0.156950824295442(02)	0.166816390476960(00)
115	0.158625229050238(02)	0.168073070300110(00)
116	0.160312461525285(02)	0.169382508035034(00)
117	0.162013067063404(02)	0.170748313680970(00)
118	0.163727628899143(02)	0.172174463216932(00)
119	0.165456772060003(02)	0.173665348179044(00)
120	0.167201167804732(02)	0.175225833763597(00)
121	0.168961538692596(02)	0.176861327253247(00)
122	0.170738664397687(02)	0.178577859018452(00)
123	0.172533388407672(02)	0.180382178934597(00)
124	0.174346625778456(02)	0.182281871825591(00)
125	0.176179372157181(02)	0.184285496561106(00)
126	0.178032714338727(02)	0.186402754789126(00)
127	0.179907842689313(02)	0.188644697109744(00)
128	0.181806065860659(02)	0.191023976978230(00)
129	0.183728828337200(02)	0.193555166047093(00)
130	0.185677731518488(02)	0.196255149430925(00)
131	0.187654559255524(02)	0.199143626135969(00)
132	0.189661309057773(02)	0.202243749608365(00)
133	0.191700230603538(02)	0.205582957548059(00)
134	0.193773873776303(02)	0.209194061259533(00)
135	0.195885149301395(02)	0.213116696892843(00)
136	0.198037406311253(02)	0.217399290756593(00)
137	0.200234533054717(02)	0.222101770233716(00)
138	0.202481089876033(02)	0.227299381784612(00)
139	0.204782488204038(02)	0.233088197222952(00)
140	0.207145236844350(02)	0.239593274571523(00)

N = 300

i	X_i^n	$W_n'(X_i^n)$
141	0.2095772896860 28(02)	0.246981143711762(00)
142	0.212088551634067(02)	0.25547963783098 9(00)
143	0.214691641842953(02)	0.265410837729415(00)
144	0.217403096897619(02)	0.277248880006507(00)
145	0.220245374502475(02)	0.291728583477932(00)
146	0.223250433947069(02)	0.310068415302829(00)
147	0.226566766671338(02)	0.334485907606618(00)
148	0.229975174638731(02)	0.369610062921528(00)
149	0.233932352310660(02)	0.427548197749874(00)
150	0.23874809763694 2(02)	0.558597792972507(00)